January 1, 2008

Asymptotic Analysis of the Selective Dip Coating of Power-Law Fluids

N Tiwari
JM Davis

Asymptotic analysis of the selective dip coating of power-law fluids

Naveen Tiwari and Jeffrey M. Davis

Citation: Physics of Fluids (1994-present) **20**, 022102 (2008); doi: 10.1063/1.2842378
View online: http://dx.doi.org/10.1063/1.2842378
View Table of Contents: http://scitation.aip.org/content/aip/journal/pof2/20/2?ver=pdfcov
Published by the AIP Publishing

Asymptotic analysis of the selective dip coating of power-law fluids

Naveen Tiwari and Jeffrey M. Davis[a)]
Department of Chemical Engineering, University of Massachusetts, Amherst, Massachusetts 01003, USA

(Received 7 August 2007; accepted 18 January 2008; published online 25 February 2008)

The dip coating of a chemically micropatterned surface bearing alternating wetting and nonwetting vertical strips is analyzed for a non-Newtonian power-law fluid. Asymptotic matching is used to determine the thickness of liquid films deposited on the $O(10\ \mu\mathrm{m})$ strips at small capillary and Bond numbers. The chemical patterning that confines the fluid laterally induces a significant transverse curvature of the free-surface. The streamwise variation in this transverse curvature along the strip provides an additional contribution to the capillary pressure gradient that is not present for uniform surfaces. Consequently, the difference in the thickness of the deposited liquid film relative to a Newtonian fluid is significantly less than for homogeneous plates or fibers. © *2008 American Institute of Physics*. [DOI: 10.1063/1.2842378]

I. INTRODUCTION

Dip coating is a simple technique for depositing thin liquid films on solid surfaces by withdrawing a substrate from a liquid reservoir. The dip coating of uniformly wetting surfaces has been analyzed extensively. Landau and Levich[1] first derived an expression for the film thickness, i.e., h_∞, of a Newtonian liquid deposited on a flat substrate withdrawn at velocity U from a reservoir of liquid with density ρ, viscosity μ, and surface tension σ,

$$h_\infty = 0.946 L_c\, \mathrm{Ca}^{2/3}, \tag{1}$$

$L_c \equiv (\sigma/\rho g)^{1/2}$ is the capillary length, and g is the acceleration of gravity. This result is restricted to small values of the capillary number; i.e., $\mathrm{Ca} = \mu U/\sigma \ll 1$. Wilson[2] later used a more formal analysis based on matched asymptotic expansions to make clear the restriction of the theory to small capillary numbers and derived an $O(\mathrm{Ca})$ correction term to the film thickness in Eq. (1) to account for gravity.

Recently, the dip-coating technique has been used to achieve selective material deposition on chemically micropatterned surfaces[3] for micro- and nanotechnology applications.[4,5] Darhuber *et al.*[3] performed careful experimental studies and a scaling analysis of the selective dip coating of a Newtonian liquid onto a vertical, wetting microstripe of width $\tilde{W}$ in the 1 to 100 μm range surrounded by nonwetting regions in the limit of small Bond number; i.e., $\mathrm{Bo} \equiv \rho g \tilde{W}^2/\sigma \ll 1$. The chemical patterning confines the liquid entirely to the wetting stripe, thereby inducing a significant transverse curvature of the free surface, which causes significant deviations from the dip coating of uniform surfaces. Davis[6] subsequently performed a theoretical analysis of this problem. He derived an equation for the centerline thickness of the liquid film deposited on the wetting stripes,[6]

$$h_\infty = 1.006\, W\, \mathrm{Ca}^{1/3}, \tag{2}$$

where $W = \tilde{W}/\sqrt{8}$. Equation (2) is valid for small capillary numbers, i.e., $\mathrm{Ca} \ll 1$ [such that terms of $O(\mathrm{Ca}^{2/3})$ are neglected], and narrow strips, i.e., $\mathrm{Bo} \ll \mathrm{Ca}^{-1/3}$, and its predictions are within about 1% of experimental measurements.[3] It was noted by Davis[6] that fluid confinement due to chemical micropatterning introduces a significant streamwise variation in the transverse curvature of the free surface in the dynamic meniscus. The associated capillary pressure gradient, which is not present for homogeneous plates or fibers, is responsible for the difference in the exponent of the capillary number relative to Eq. (1). [The change in the characteristic length scale from the O(mm) capillary length to the $O(\mu\mathrm{m})$ strip width is analogous to the introduction of the fiber radius for the dip coating of a thin fiber.[7]] An extension of the work was presented by Tiwari and Davis,[8] who analyzed the effect of insoluble surfactant on selective dip coating.

Studies of dip-coating uniform surfaces and the related motion of long gas bubbles in liquid-filled capillary tubes[9] have also been extended to non-Newtonian liquids,[10–13] but no such work exists for micropatterned surfaces. The experimental work of Siau *et al.*[14] on the dip coating of dielectric and solder mask epoxy polymer layers forms a motivation for considering the dip coating of non-Newtonian fluids onto such chemically micropatterned surfaces. This analysis is focused on determining how the additional capillary term from lateral fluid confinement interacts with the non-Newtonian rheology to affect the thickness of the deposited liquid film.

II. ANALYSIS

Consider the selective dip coating of an incompressible, non-Newtonian fluid onto a chemically micropatterned plate. The plate is withdrawn out of a liquid reservoir in the negative x direction, as shown in Fig. 1. The coordinate z is directed outwardly normal from the substrate. The film can be characterized by three regions based on the controlling forces. In the lubrication film region, all streamwise gradients vanish. The film-thickness is given by the (unknown) constant h_∞, which will be determined through asymptotic matching in the dynamic meniscus. Near the liquid reservoir, the balance of capillary terms and possibly gravity forms the static meniscus. In the dynamic meniscus region, capillary

a)Electronic mail: jmdavis@ecs.umass.edu.

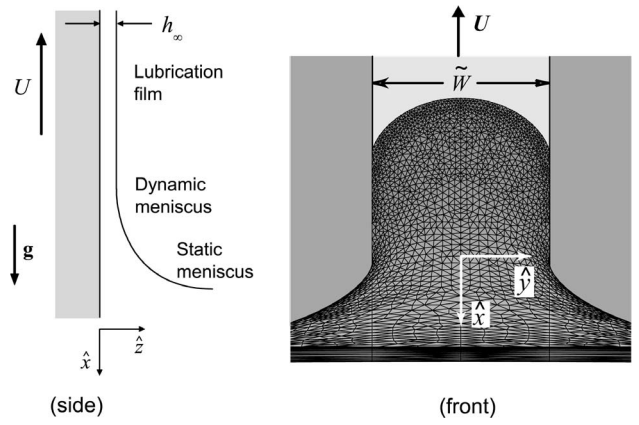

FIG. 1. Diagram of the dip-coating process and meniscus profile on a (stationary) micropatterned plate immersed in a liquid bath. As the plate is withdrawn, liquid is entrained on the vertical, wetting strip of width $\tilde{W}$ [$O(10\ \mu\text{m})$], while no liquid is entrained on the surrounding nonwetting regions.

forces balance the viscous forces. This region asymptotically matches the constant-film region and the static meniscus region.

The fluid is assumed to follow power-law behavior such that viscous stresses are related to the rate of strain through the Ostwald–de Waele model,[15] i.e., $\boldsymbol{\tau}=2m(2\Gamma)^{n-1}\boldsymbol{\Gamma}$, where $\boldsymbol{\tau}$ is the viscous stress tensor, m is a positive constant, n is the power-law index, $\boldsymbol{\Gamma}$ is the rate-of-strain tensor, and $\Gamma=(1/2\boldsymbol{\Gamma}:\boldsymbol{\Gamma})^{1/2}$. Shear thinning behavior is obtained for $n<1$, Newtonian behavior for $n=1$, and shear thickening behavior for $n>1$. For the power-law fluid, the capillary number is defined as $\text{Ca}=\mu_0 U/\sigma$, where the reference viscosity $\mu_0=m(U/W)^{n-1}$ for a micropatterned surface or $\mu_0^u=m(U/L_c)^{n-1}$ for a uniform surface. This definition differs from that used in previous studies[16] that employed the unknown film thickness h_∞ as the length scale in the reference viscosity μ_0. This analysis instead uses W or L_c, which can be calculated *a priori* from the physical properties of the liquid.

With the restriction of small capillary number, the flow is described by the lubrication approximation

$$-\frac{\partial p}{\partial x}+\rho g+\frac{\partial}{\partial z}\left[m\left(\frac{\partial u}{\partial z}\right)^n\right]=0. \tag{3}$$

The momentum equations can be formally reduced to Eq. (3) by neglecting terms of $O[\text{Re}\,\text{Ca}^{(n+1)/(n+2)}]$ and $O[\text{Ca}^{2/(n+2)}]$, where $\text{Re}=\rho WU/\mu_0$ is the Reynolds number. This reduction is a straightforward extension of the microstripe analysis that has been presented for a Newtonian fluid.[8] Neglecting viscous stresses at $O[\text{Ca}^{2/(n+2)}]$, the normal stress balance specifies the capillary pressure,

$$-p=\sigma(2\kappa)=-\sigma\nabla_s\cdot\boldsymbol{n}\approx\sigma(h_{xx}+h_{yy}), \tag{4}$$

where 2κ is the mean curvature of the free surface at $z=h(x,y)$ and $\boldsymbol{n}$ is the unit normal vector at $z=h$. Equation (3) is subject to the boundary conditions of no slip at the solid-liquid interface,

$$\boldsymbol{u}=-U\boldsymbol{e}_x \quad \text{at} \quad z=0, \tag{5}$$

and vanishing shear stress at the liquid-air interface,

$$\partial u/\partial z=0 \quad \text{at} \quad z=h(x,y). \tag{6}$$

The velocity u is found by integrating Eq. (3) and using the boundary conditions given in Eqs. (5) and (6). A further integration with respect to z yields the flux, which is equated to its asymptotic value as $x\to-\infty$ to give

$$h_{xxx}+h_{yyx}=-\frac{\rho g}{\sigma}+\left[b\left(\frac{m^{1/n}U}{\sigma^{1/n}}\right)\left(\frac{h-h_\infty}{h^b}\right)+\left(\frac{\rho g}{\sigma}\right)^{1/n}\left(\frac{h_\infty}{h}\right)^b\right]^n, \tag{7}$$

where $h\to h_\infty$ as $x\to-\infty$ and $b\equiv(2n+1)/n$.

A. Wide stripes

In the dynamic meniscus, the variables can be made dimensionless for wide stripes using scales motivated by the analysis for a uniformly wetting plate.[10] Introducing the variables $\hat{h}=h/(L_c\delta^2)$, $\hat{x}=x/(L_c\delta)$, and $\hat{y}=y/W$ into Eq. (7), where $\delta\equiv\text{Ca}^{1/(2n+1)}\ll1$, yields

$$\hat{h}_{\hat{x}\hat{x}\hat{x}}+\text{Bo}^{-1}\delta^2\hat{h}_{\hat{y}\hat{y}\hat{x}}=-\delta+\left[b\left(\frac{\hat{h}-\hat{h}_\infty}{\hat{h}^b}\right)+\delta^{1/n}\left(\frac{\hat{h}_\infty}{\hat{h}}\right)^b\right]^n. \tag{8}$$

Here, $\text{Bo}\equiv(W/L_c)^2=\rho gW^2/\sigma$ is the Bond number. If $\text{Bo}^{-1}\delta^2\ll1$, which corresponds to stripes much wider than the dynamic capillary length ($L_c\delta$), then the second term on the left-hand side of Eq. (8) is negligible, and the leading-order solution for a uniform plate is recovered. Neglecting the small terms ($\text{Bo}^{-1}\delta^2\ll1$, $\delta\ll1$) due to the change in transverse curvature and drainage due to gravity converts Eq. (8) to

$$\hat{h}_{\hat{x}\hat{x}\hat{x}}=\left(\frac{2n+1}{n}\right)^n\frac{(\hat{h}-\hat{h}_\infty)^n}{\hat{h}^{(2n+1)}}, \tag{9}$$

subject to the boundary condition $\hat{h}\to\hat{h}_\infty$ as $\hat{x}\to-\infty$. As $\hat{x}\to\infty$, $\hat{h}_{\hat{x}\hat{x}}\to a$, which is a constant that can be found by integrating Eq. (9) numerically. Equating this constant, limiting curvature of the lubrication film region with the limiting curvature of the hydrostatic meniscus (in a common set of scaled variables) completes the matching process in the overlap region and specifies the deposited film thickness, which has been computed by a number of authors for different scalings.[16]

B. Narrow stripes

Now consider the limit of narrow stripes, which corresponds to $\text{Bo}=O(\delta^2)$ or smaller. The reference viscosity used in the definition of the capillary number for these narrow stripes is $\mu_0=m(U/W)^{n-1}$. With the restriction $\epsilon^2\equiv\text{Ca}^{2/(n+2)}\ll1$, an $\hat{x}=$const cross section of the free surface of the liquid along the microstripe must be an arc of a circle,[8] which simplifies to a parabola at the same order of approximation.

Introducing the substitution $h(x,y)=h_0(x)[1-4(y/\tilde{W})^2]$ into Eq. (7) reduces the analysis to a one-dimensional matching problem to determine h_0, the film thickness along the centerline of the stripe, which is governed by

$$h_{0xxx} - W^{-2}h_{0x} = -\frac{\rho g}{\sigma} + \left[b\left(\frac{m^{1/n}U}{\sigma^{1/n}}\right)\left(\frac{h_0 - h_{0\infty}}{h_0^b}\right) + \left(\frac{\rho g}{\sigma}\right)^{1/n}\left(\frac{h_{0\infty}}{h_0}\right)^b \right]^n, \tag{10}$$

where $h_0 \to h_{0\infty}$ as $x \to -\infty$.

For these narrow stripes, the transverse curvature of the liquid ribbon is significant, and Eq. (10) must be scaled such that both capillary terms are comparable to the viscous terms. Introducing the new variables $\xi = x/W$ and $\eta = h_0/(\epsilon W)$ transforms Eq. (10) into

$$\eta_{\xi\xi\xi} - \eta_\xi = \left(\frac{2n+1}{n}\right)^n \frac{(\eta - \eta_\infty)^n}{\eta^{2n+1}}, \tag{11}$$

where gravity has been neglected at $O(\mathrm{Bo}\,\epsilon^{-1})$. Equation (11) is subject to the boundary condition $\eta \to \eta_\infty$ as $\xi \to -\infty$. As $\xi \to \infty$, $\eta_{\xi\xi} - \eta \to C_S$, which is a constant found by numerically integrating Eq. (11). The numerical value of the constant η_∞ is determined such that C_S is equal to the limiting curvature of the meniscus.

In the meniscus region, W is the appropriate scale for all coordinates.[6] Introducing the new variables $H = h/W$, $X = x/W$, $Y = \hat{y}/W$, and $\bar{\boldsymbol{u}} = \boldsymbol{u}/U$ into the momentum equation, the curvature in the static meniscus is governed by

$$\frac{\partial(2\kappa)}{\partial x} = -\mathrm{Bo} + \mathrm{Re}\,\mathrm{Ca}\,\boldsymbol{e}_x \cdot (\bar{\boldsymbol{u}} \cdot \nabla\bar{\boldsymbol{u}}) - \mathrm{Ca}\,\boldsymbol{e}_x \cdot (\nabla \cdot \boldsymbol{\tau}). \tag{12}$$

The constraints imposed in the dynamic meniscus region require that all terms on the right-hand side are small, so the shape of the meniscus is not influenced by the motion of the plate or by gravity at leading order. The mean curvature of the meniscus therefore reduces to $2\kappa = 0$, and the exact meniscus profile need not be determined explicitly.[6]

Evaluating 2κ along the centerline of the stripe ($y=0$) and noting that the free surface must be symmetric (and that $h_x \to 0$ at the top of the static meniscus to match the dynamic meniscus) reveals that $H_{XX} + H_{YY} \to C_M = 0$ is the limiting behavior at the top of the static meniscus to which the solution in the dynamic meniscus should be matched. With $C_S = C_M = 0$, the resulting matching condition formulated for the dynamic meniscus is

$$\eta_{\xi\xi} - \eta \to 0 \quad \text{as} \quad \xi \to \infty. \tag{13}$$

The physical interpretation of Eq. (13) is that the mean curvature of the film asymptotes to zero as the static meniscus is approached from above. In the scaled variables appropriate to the dynamic meniscus, $\eta_{\xi\xi}$ represents the streamwise curvature, and $-\eta$ the transverse curvature induced by fluid confinement to the microstripe. The deposited film thickness is found by numerically integrating Eq. (11) via a standard shooting method for a value of η_∞ until Eq. (13) is satisfied. The MATLAB function *ode45* was used for the numerical integration with linearization about the solution $\eta = \eta_\infty$ used for the initial condition.

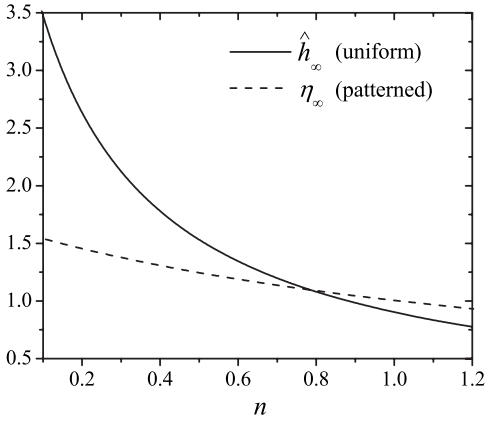

FIG. 2. Variation of the numerical prefactor in Eqs. (14) and (15) with the power-law index n for both uniform and micropatterned surfaces.

III. RESULTS

For the chemically micropatterned surface, the centerline film thickness is predicted to be

$$h_\infty = \eta_\infty \epsilon W = \eta_\infty W\,\mathrm{Ca}^{1/(n+2)}. \tag{14}$$

A similar integration of Eq. (9), with $a = \sqrt{2}$, yields a prediction for the thickness of the film deposited on a uniformly wetting surface,

$$h_\infty = \hat{h}_\infty L_c \mathrm{Ca}^{2/(2n+1)}, \tag{15}$$

which is consistent with published results using different scalings.[10,16] Calculated values of the prefactors η_∞ and $\hat{h}_\infty$ are plotted versus n in Fig. 2 for uniform and micropatterned surfaces for the range of power-law exponents $n = 0.1-1.2$, which shows that η_∞ varies more weakly with n than does $\hat{h}_\infty$. These curves can be approximated by a reciprocal function fit that relates the prefactor to the power-law index. For the micropatterned surface, $\eta_\infty \approx (0.611 + 0.385n)^{-1}$. For a uniform surface, $\hat{h}_\infty \approx (0.202 + 0.906n)^{-1}$.

The difference in the exponent of Ca in Eqs. (14) and (15) relative to that of a Newtonian fluid [Eqs. (1) and (2)] is plotted versus n in Fig. 3. This difference is $\alpha = 1/(n+2) - 1/3$ for a micropatterned surface and $\alpha = 2/(2n+1) - 2/3$ for a uniform surface. In this regime of low capillary number, the variation of the exponent with n has a much more significant influence on the deposited film thickness than does the numerical prefactor $\eta_\infty(n)$. Because α is much closer to zero for any n for a micropatterned surface, the variation of h_∞ with n is much weaker than for a uniform surface for a given Ca. Taken together, the results plotted in Figs. 2 and 3 indicate that the deposited film thickness for a power-law fluid remains much closer to that for Newtonian fluid on a micropatterned surface than on a uniform surface. The trends in Figs. 2 and 3 are consistent with those observed experimentally for the withdrawal of a vertical tube from a non-Newtonian liquid by Huzyak and Koelling[13] in

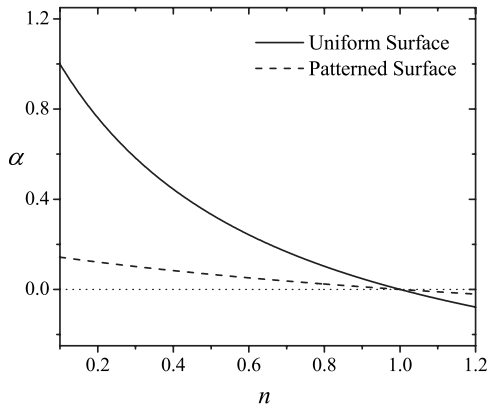

FIG. 3. Comparison of the exponent of the capillary number in the expressions for the deposited film thickness [Eqs. (14) and (15)] for the uniform and micropatterned surfaces. The difference in the exponent of the capillary number relative to a Newtonian fluid is $\alpha=1/(n+2)-1/3$ for a micropatterned surface and $\alpha=2/(2n+1)-2/3$ for a uniform surface.

that the numerical prefactor η_∞ increases as the power-law index decreases (while the dimensional film thickness $\hat{h}_\infty$ decreases due to the dependence of Ca on n).

The weaker dependence of h_∞ on n for a micropatterned surface is due to the presence of the additional $O(1)$ capillary term η_ξ in Eq. (11), which results from the streamwise variation of the transverse curvature of the free surface along the microstripe. [The comparable term in Eq. (9) is $O(\mathrm{Bo}^{-1}\delta^2)$, where $\mathrm{Bo}^{-1}\delta^2 \ll 1$.] This term is the only difference between Eqs. (11) and (9) and diminishes the influence of the viscous terms. For a Newtonian fluid, this additional term weakens the dependence of h_∞ on Ca [1/3 in Eq. (2) versus 2/3 in Eq. (1)]. For a power-law fluid, this term further weakens the dependence of h_∞ on n through both η_∞ and α, as shown in Figs. 2 and 3.

The dependence of h_∞ on n is therefore much weaker when the capillary term from lateral fluid confinement is significant, which is seen from Eq. (8) to require $\mathrm{Bo}^{-1}\delta^2 = O(1)$ or larger (if $\mathrm{Bo}^{-1}\delta^2 \gg 1$, then W replaces δ as the streamwise length scale, and both capillary terms remain the same order). If $\mathrm{Bo}^{-1}\delta^2 \ll 1$, then the capillary term from fluid confinement is negligible, and h_∞ has the same strong dependence on n as for uniform surfaces.

IV. CONCLUSIONS

This analysis for a microstripe is similar to that for a thin, cylindrical fiber in that the stripe width or fiber radius controls the meniscus curvature and replaces the capillary length as the length scale in Eq. (14). The key difference is that the transverse curvature induced by micropatterning changes in the x direction along the microstripe, as represented by the $W^{-2}h_{0x}$ term in Eq. (10), which makes an important contribution to the streamwise capillary pressure gradient. The change in the streamwise curvature (h_{0xxx}) drains fluid from the stripe, while the change in the transverse curvature effectively forces liquid up from the meniscus (along with the viscous terms, which have the same sign). Unlike the withdrawal of a fiber, h_{0xx} does not approach a constant as $x \to -\infty$. Instead, the total curvature (represented by $h_{0xx} - W^{-2}h_0$) matches the full curvature of the meniscus. The competition between the two capillary terms leads to a reduction in the effect of the power-law index on the thickness of the deposited film relative to a uniform surface.

For a thin fiber, by contrast, the term corresponding to the pressure induced by the curvature of the free surface in the direction transverse to flow is a constant until $O(\delta^2)$.[7] To the first order of approximation its derivative is zero, and there is no resulting dynamical effect. With an appropriate change in variables, the governing equation for a thin cylinder in the dynamic meniscus thus reduces to Eq. (9) for a uniform plate. The change in streamwise curvature is balanced only by the viscous terms, which leads to a stronger dependence on the capillary number in Eq. (1) versus Eq. (2) and a stronger dependence on the power-law index n in Eq. (15) versus Eq. (14).

ACKNOWLEDGMENTS

The authors gratefully acknowledge financial support from a 3M Nontenured Faculty Grant.

[1] L. D. Landau and B. V. G. Levich, "Dragging of a liquid by a moving plate," Acta Physicochim. URSS **17**, 42 (1942).
[2] S. D. R. Wilson, "The drag-out problem in film coating theory," J. Eng. Math. **16**, 209 (1982).
[3] A. A. Darhuber, S. M. Troian, J. M. Davis, S. M. Miller, and S. Wagner, "Selective dip-coating of chemically micropatterned surfaces," J. Appl. Phys. **88**, 5119 (2000).
[4] D. Qin, Y. Xia, B. Xu, H. Yang, C. Zhu, and G. M. Whitesides, "Fabrication of ordered two-dimensional arrays of micro- and nanoparticles using patterned self-assembled monolayers as templates," Adv. Mater. (Weinheim, Ger.) **11**, 1433 (1999).
[5] H. Y. Fan, Y. F. Lu, A. Stump, S. T. Reed, T. Baer, R. Schunk, V. Perez-Luna, G. P. Lopez, and C. J. Brinker, "Rapid prototyping of patterned functional nanostructures," Nature (London) **405**, 56 (2000).
[6] J. M. Davis, "Asymptotic analysis of liquid films dip-coated onto chemically micropatterned surfaces," Phys. Fluids **17**, 038101 (2005).
[7] S. D. R. Wilson, "Coating flow on to rods and wires," AIChE J. **34**, 1732 (1988).
[8] N. Tiwari and J. M. Davis, "Theoretical analysis of the effect of insoluble surfactant on the dip coating of chemically micropatterned surfaces," Phys. Fluids **18**, 022102 (2006).
[9] F. P. Bretherton, "The motion of long bubbles in tubes," J. Fluid Mech. **10**, 166 (1961).
[10] C. Gutfinger and J. A. Tallmadge, "Film of non-Newtonian fluids adhering to flat plates," AIChE J. **11**, 403 (1965).
[11] R. P. Spiers, C. V. Subbaraman, and W. L. Wilkinson, "Free coating of a non-Newtonian liquid onto a vertical surface," Chem. Eng. Sci. **30**, 379 (1975).
[12] J. S. Ro and G. M. Homsy, "Viscoelastic free surface flows: thin film hydrodynamics of Hele-Shaw and dip-coating flows," J. Non-Newtonian Fluid Mech. **57**, 203 (1995).
[13] P. C. Huzyak and K. W. Koelling, "The penetration of a long bubble through a viscoelastic fluid in a tube," J. Non-Newtonian Fluid Mech. **71**, 73 (1997).
[14] S. Siau, A. Vervaet, S. Degrande, E. Schacht, and A. V. Calster, "Dip coating of dielectric and solder mask epoxy polymer layers for build-up purposes," Appl. Surf. Sci. **245**, 353 (2005).
[15] R. B. Bird, R. C. Armstrong, and O. Hassager, *Dynamics of Polymeric Liquids* (Wiley, New York, 1977).
[16] S. J. Weinstein and K. J. Ruschak, "Coating flows," Annu. Rev. Fluid Mech. **36**, 29 (2004).